DARK MATTER 101

DARK MATTER 101

From production to detection

David G. Cerdeño

Durham University

CONTENTS

CHAPTER 1

MOTIVATION FOR DARK MATTER

The existence of a vast amount of dark matter (DM) in the Universe is supported by many astrophysical and cosmological observations. The latest measurements indicate that approximately a 27% of the Universe energy density is in form of a new type of non-baryonic cold DM. Given that the Standard Model (SM) of particle physics does not contain any viable candidate to account for it, DM can be regarded as one of the clearest hints of new physics.

1.1 Motivation for Dark Matter

Astrophysical and cosmological observations have provided substantial evidence that point towards the existence of vast amounts of a new type of matter, that does not emit or absorb light. All astrophysical evidence for DM is solely based on gravitational effects (either trough the observation of dynamical effects, deflection of light by gravitational lensing or measurements of the gravitational potential of galaxy clusters), which cannot be accounted for by just the observed luminous matter. The simplest way to solve these problems is the inclusion of more matter (which does not emit light - and is therefore dark in the astronomical sense[1]). Modifications in the Newtonian equation relating force and accelerations have also been suggested to address the problem at galactic scales, but this hypothesis is

[1] Since dark matter does not absorb light, a more adequate name would have been transparent matter.

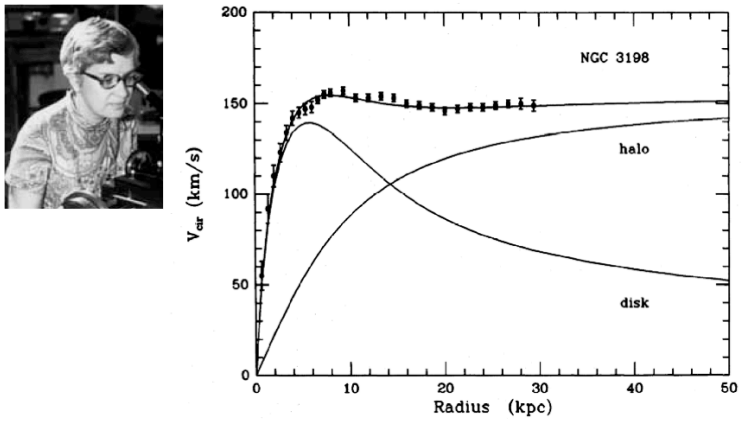

Figure 1.1 Left) Vera Rubin. Right) Rotation curve of a spiral galaxy, where the contribution from the luminous disc and dark matter halo is shown by means of solid lines.

insufficient to account for effects at other scales (e.g., cluster of galaxies) or reproduce the anisotropies in the CMB.

No known particle can play the role of the DM (we will later argue that neutrinos contribute to a small part of the DM). Thus, this is one of the clearest hints for Physics Beyond the Standard Model and provides a window to new particle physics models. In the following I summarise some of the main pieces of evidence for DM at different scales.

I recommend completing this section with the first chapters of Ref. [1] and the recent article [2].

1.1.1 Galactic scale

Rotation curves of spiral galaxies Rotation curves of spiral galaxies are probably the best-known examples of how the dynamical properties of astrophysical objects are affected by DM. Applying Gauss' Law to a spiral galaxy (one can safely ignore the contribution from the spiral arms and assume a spherical distribution of matter in the bulge) leads to a simple relation between the rotation velocity of objects which are gravitationally bound to the galaxy and their distance to the galactic centre:

$$v = \sqrt{\frac{GM(r)}{r}} \,, \tag{1.1}$$

where $M(r)$ is the mass contained within the radius r. In the outskirts of the galaxy, where we expect that M does not increase any more, we would therefore expect a decay $v_{rot} \propto r^{-1/2}$.

Vera Rubin's observations of rotation curves of spiral galaxies [3, 4] showed a very slow decrease with the galactic radius. The careful work of Bosma [5], van Albada and Sancisi [6] showed that this flatness could not be accounted for by simply modifying the relative weight of the diverse galactic components (bulge, disc, gas), a new component was needed with a different spatial distribution (see Fig. 1.1).

Notice that the flatness of rotation curves can be obtained if a new mass component is introduced, whose mass distribution satisfies $M(r) \propto r$ in eq.(1.1). This is precisely the

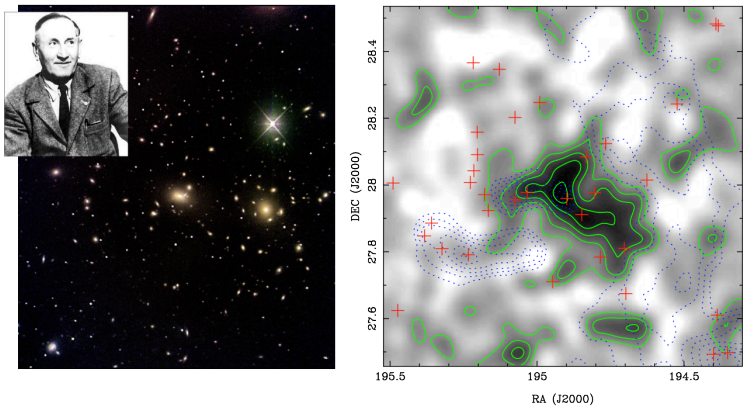

Figure 1.2 Left) Coma cluster and F. Zwicky, who carried out measurements of the peculiar velocities of this object. Right) Modern techniques [7], based on gravitational lensing, allow for a much more precise determination of the total mass of this object.

relation that one expects for a self-gravitational gas of non-interacting particles. This halo of DM can extend up to ten times the size of the galactic disc and contains approximately an 80% of the total mass of the galaxy.

Since then, flat rotation curves have been found in spiral galaxies, further strengthening the DM hypothesis. Of course, our own galaxy, the Milky Way is no exception. N-body simulations have proved to be very important tools in determining the properties of DM haloes. These can be characterised in terms of their density profile $\rho(r)$ and the velocity distribution function $f(v)$. Observations of the local dynamics provide a measurement of the DM density at our position in the Galaxy. Up to substantial uncertainties, the local DM density can vary in a range $\rho_0 = 0.2 - 1$ GeV cm^{-3}. It is customary to describe the DM halo in terms of a Spherical Isothermal Halo, in which the velocity distribution follows a Maxwell-Boltzmann law, but deviations from this are also expected. Finally, due to numerical limitations, current N-body simulations cannot predict the DM distribution at the centre of the galaxy. Whereas some results suggest the existence of a cusp of DM in the galactic centre, other simulations seem to favour a core. Finally, the effect of baryons is not easy to simulate, although substantial improvements have been recently made.

Local probes

1.1.2 Galaxy Clusters

Peculiar motion of clusters. Fritz Zwicky studied the peculiar motions of galaxies in the Coma cluster [8, 9]. The aim was to measure the total mass of the system through a method that did not rely only on the information from visible objects, and thus included also the faint and non-luminous components). Assuming that the galaxy cluster is an isolated system, the virial theorem can be used to relate the average velocity of objects with the gravitational potential (or the total mass of the system).

As in the case of galaxies, this determination of the mass is insensitive to whether objects emit any light or not. This can then be contrasted with other determinations that are based on the luminosity. The results showed an extremely large mass-to-light ratio, indica-

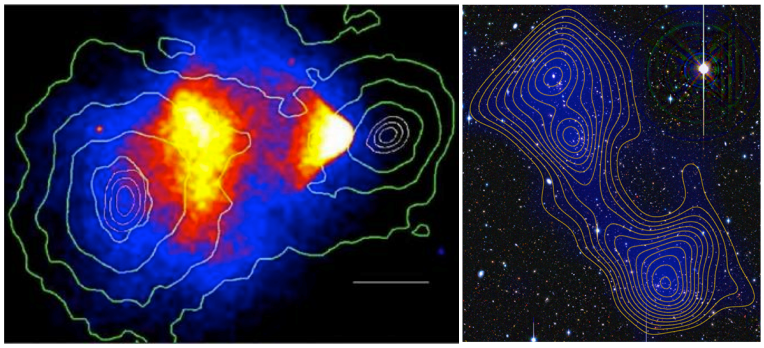

Figure 1.3 Left) Deep Chandra image of the Bullet cluster. Green lines represent mass contours from weak lensing. Right) Dark filament in the system Abell 222/223, reconstructed using weak lensing.

tive of the existence of large amounts of missing mass, which can be attributed to a DM component.

Modern determinations through weak lensing techniques provide a better gravitational determination of the cluster masses [10, 7] (see Fig. 1.2). I recommend reading through Ref.[9] for a derivation of the virial theorem in the context of Galaxy clusters.

Dynamical systems. The Bullet Cluster (1E 0657-558) is a paradigmatic example of the effect of dark matter in dynamical systems. It consists of two galaxy clusters which underwent a collision. The visible components of the cluster, observed by the Chandra X-ray satellite, display a characteristic shock wave (which gives name to the whole system). On the other hand, weak-lensing analyses, which make use of data from the Hubble Space Telescope, have revealed that most of the mass of the system is displaced from the visible components. The accepted interpretation is that the dark matter components of the clusters have crossed without interacting significantly (see e.g., Ref. [11, 12]).

The Bullet Cluster is considered one of the best arguments against MOND theories (since the gravitational effects occur where there is no visible matter). It also sets an upper bound on the self-interaction strength of dark matter particles.

DM filaments. Observations of the distribution of luminous matter at large scales have shown that it follows a filamentary structure. Numerical simulations of structure formation with cold DM have been able to reproduce this feature. To date, it is well understood that DM plays a fundamental role in creating that filamentary network, gravitationally trapping the luminous matter. Recently, the comparison of the distribution of luminous matter in the Abell 222/223 supercluster with weak-lensing data has shown the existence of a dark filament joining the two clusters of the system. That filament, having no visible counterpart, is believed to be made of DM.

1.1.3 Cosmological scale

Finally, DM has also left its footprint in the anisotropies of the Cosmic Microwave Background (CMB). The analysis of the CMB constitutes a primary tool to determine the cosmological parameters of the Universe. The data obtained by dedicated satellites in the past

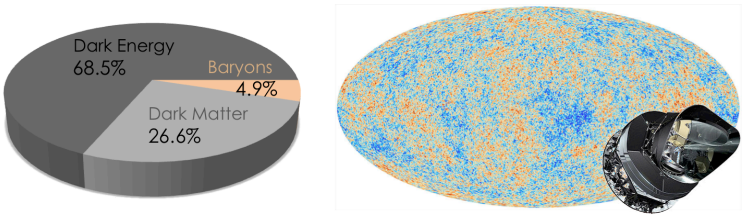

Figure 1.4 Left) Contribution to the energy density for each of the components of the Universe. Right) Planck temperature map.

decades has confirmed that we live in a flat Universe (COBE), dominated by dark matter and dark energy (WMAP), whose cosmological abundances have been determined with great precision (Planck).

The abundance of DM is normally expressed in terms of the cosmological density parameter, defined as $\Omega_{DM}h^2 = \rho_{DM}/\rho_c$ where ρ_c is the critical density necessary to recover a flat Universe and $h = 0.7$ is the normalised Hubble parameter. The most recent measurements by the Planck satellite, combined with data obtained from Supernovae (that trace the Universe expansion) yield

$$\Omega_{CDM}h^2 = 0.1196 \pm 0.0031 \, . \tag{1.2}$$

Given that $\Omega \approx 1$, this means that dark matter is responsible for approximately a 26% of the Universe energy density nowadays. Even more surprising is the fact that another exotic component is needed, *dark energy*, which makes up approximately the 69% of the total energy density (see Fig. 1.4).

1.2 Dark Matter properties

1.2.1 NonBaryonic

The results of the CMB, together with the predictions from Big Bang nucleosynthesis, suggest that only $4 - 5\%$ of the total energy budget of the universe is made out of ordinary (baryonic) matter. Given the mismatch of this with the total matter content, we must conclude that DM is non-baryonic.

Neutrinos. Neutrinos deserve special mention in this section, being the only viable non-baryonic DM candidate within the SM. Neutrinos are very abundant particles in the Universe and they are known to have a (very small) mass. Given that they also interact very feebly with ordinary matter (only through the electroweak force) they are in fact a component of the DM. There are, however various arguments that show that they contribute in fact to a very small part.

First, neutrinos are *too light*. Through the study of the decoupling of neutrinos in the early universe we can compute their thermal relic abundance. Since neutrinos are relativistic particles at the time of decoupling, this is in fact a very easy computation (we will come back to this in Section 2.2.1), and yields

$$\Omega_\nu h^2 \approx \frac{\sum_i m_i}{91\,\mathrm{eV}} \, . \tag{1.3}$$

Using current upper bounds on the neutrino mass, we obtain $\Omega_\nu h^2 < 0.003$, a small fraction of the total DM abundance.

Second, neutrinos are *relativistic* (hot) at the epoch of structure formation. As mentioned above, hot DM leads to a different hierarchy of structure formation at large scales, with large objects forming first and small ones occurring only after fragmentation. This is inconsistent with observations.

1.2.2 Neutral

It is generally argued that DM particles must be electrically neutral. Otherwise they would scatter light and thus not be dark. Similarly, constrains on charged DM particles can be extracted from unsuccessful searches for exotic atoms. Constraints on heavy millicharged particles are inferred from cosmological and astrophysical observations as well as direct laboratory tests [13, 14, 15]. Millicharged DM particles scatter off electrons and protons at the recombination epoch via Rutherford-like interactions. If millicharged particles couple tightly to the baryonphoton plasma during the recombination epoch, they behave like baryons thus affecting the CMB power spectrum in several ways [13, 14]. For particles much heavier than the proton, this results in an upper bound of its charge ϵ [14]

$$\epsilon \leq 2.24 \times 10^{-4} \, (M/1\,\mathrm{TeV})^{1/2} \, . \tag{1.4}$$

Similarly, direct detection places upper bounds on the charge of the DM particle [16]

$$\epsilon \leq 7.6 \times 10^{-4} \, (M/1\,\mathrm{TeV})^{1/2} \, . \tag{1.5}$$

1.2.3 Nonrelativistic

Numerical simulations of structure formation in the Early Universe have become a very useful tool to understand some of the properties of dark matter. In particular, it was soon found that dark matter has to be non-relativistic (cold) at the epoch of structure formation. Relativistic (hot) dark matter has a larger free-streaming length (the average distance traveled by a dark matter particle before it falls into a potential well). This leads to inconsistencies with observations.

However, at the Galactic scale, cold dark matter simulations lead to the occurrence of too much substructure in dark matter haloes. Apparently this could lead to a large number of subhaloes (observable through the luminous matter that falls into their potential wells). It was argued that if dark matter was *warm* (having a mass of approximately $2 - 3$ keV) this problem would be alleviated.

Modern simulations, where the effect of baryons is included, are fundamental in order to fully understand structure formation in our Galaxy and determine whether dark matter is cold or warm.

1.2.4 Long-lived

Possibly the most obvious observation is that DM is a long-lived (if not stable) particle. The footprint of DM can be observed in the CMB anisotropies, its presence is essential for structure formation and we can feel its gravitational effects in clusters of galaxies and galaxies nowadays.

Stable DM candidates are common in models in which a new discrete symmetry is imposed by ensuring that the DM particle is the lightest with an exotic charge (and there-

fore its decay is forbidden). This is the case, e.g., in Supersymmetry (when R-parity is imposed), Kaluza-Klein scenarios (K-parity) or little Higgs models.

However, stability is not required by observation. DM particles can decay, as long as their lifetime is longer than the age of the universe. *Long-lived* DM particles feature very small couplings. Characteristic examples are gravitinos (whose decay channels are gravitationally suppressed) or axinos (which decays through the axion coupling).

1.2.5 Collisionless

Dynamical systems, such as cluster collisions, set an upper bound to the self-interactions of DM particles. Observations seem to suggest that the DM component in these objects is mostly collision-less, thus behaving very differently than ordinary matter. Dark matter's lack of deceleration in the bullet cluster constrains its self-interaction cross-section $\sigma/m < 1.25$ cm^2 g$^{-1} \approx 2$ barn GeV^{-1}.

Notice however, that self-interacting dark matter with a cross section in the range $0.1 < \sigma/m < 1$ cm^2 g^{-1} can be very beneficial in order to alleviate the problems with the amount of substructure in numerical simulations of DM haloes.

[17]

CHAPTER 2

FREEZE OUT OF MASSIVE SPECIES

In this chapter we will address the computation of the relic abundance of dark matter particles, making special emphasis in the case of thermal production in the Early Universe.

2.1 Cosmological Preliminaries

This section does not intend to be a comprehensive review on Cosmology, but only an introduction to some of the elements that we will need for the calculation of Dark Matter freeze-out.

We can describe our isotropic and homogeneous Universe in terms of the Friedman-Lemaître-Robertson-Walker (FLRW) metric, which is exact solution of Einstein's field equations of general relativity

$$ds^2 = dt^2 - a^2(t)\left(\frac{dr^2}{1-kr^2} + r^2(d\theta^2 + \sin\theta d\phi^2)\right) = g_{\mu\nu}dx^\mu dx^\nu \,. \qquad (2.1)$$

The constant $k = \{-1, 0, +1\}$ corresponds to the spatial curvature, with $k = 0$ corresponding to a flat Universe (the choice we will be making in these notes). The affine connection, used to connect nearby tangent spaces (thus enabling the differentiation of tangent vector fields), is defined as

$$\Gamma^\mu_{\nu\lambda} = \frac{1}{2}g^{\mu\sigma}(g_{\sigma\nu,\lambda} + g_{\sigma\lambda,\nu} - g_{\nu\lambda,\sigma}) \,, \qquad (2.2)$$

These can also be found in the literature as Christoffel symbols, used in the definition of a covariant derivative. They are greatly simplified in the case of a FLRW metric, since most of the derivatives vanish.

The expansion of the Universe is controlled by the scale parameter $a(t)$. More specifically, we can define the Hubble parameter, $H \equiv \dot{a}(t)/a(t)$ (where the dot denotes time derivation), which encodes the rate at which space is expanding. In the following, we are going to work with a radiation-dominated Universe. Notice that matter-radiation equality only occurs very late (when the Universe is approximately 60 kyr) and dark matter freeze-out occurs before BBN. The Hubble parameter for a radiation-dominated Universe reads

$$H = 1.66\, g_*^{1/2}\, \frac{T^2}{M_P}\,, \tag{2.3}$$

where $M_P = 1.22 \times 10^{19}$ GeV.

It is customary to define the dimensionless parameter $x = m/T$ (where m is a mass parameter that we will later associate to the DM mass) and extract the explicit x dependence from the Hubble parameter to define $H(m)$ as follows

$$H(m) = 1.66\, g_*^{1/2}\, \frac{m^2}{M_P} = Hx^2\,. \tag{2.4}$$

In this section we will try to compute the time evolution of the number density of dark matter particles, in order to be able to compute their relic abundance today and what this implies in the interaction strength of dark matter particles. The phase space distribution function f describes the occupancy number in phase space for a given particle in *kinetic* equilibrium, and distinguishes between fermions and bosons.

$$f = \frac{1}{e^{(E-\mu)/T} \pm 1}\,, \tag{2.5}$$

where the $(-)$ sign corresponds to bosons and the $(+)$ sign to fermions. E is the energy and μ the chemical potential. For species in chemical equilibrium, the chemical potential is conserved in the interactions. Thus, for processes such as $i + j \leftrightarrow c + d$ we have $\mu_i + \mu_j = \mu_c + \mu_d$. Notice then that all chemical potentials can be expressed in terms of the chemical potentials of conserved quantities, such as the baryon chemical potential μ_B. The number of independent chemical potentials corresponds to conserved particle numbers. This implies, for example, that given a particle with μ_i, the corresponding antiparticle would have the opposite chemical potential $-\mu_i$. For the same reason, since the number of photons is not conserved in interactions, $\mu_\gamma = 0$

Using the expression of the phase space distribution function (2.5), and integrating in phase space, we can compute a series of observables in the Universe. In particular, the number density of particles, n, the energy density, ρ, and pressure, p, for a dilute and weakly-interacting gas of particles with g internal degrees of freedom read

$$n = \frac{g}{(2\pi)^3} \int f(\mathbf{p})\, d^3p, \tag{2.6}$$

$$\rho = \frac{g}{(2\pi)^3} \int E(\mathbf{p})\, f(\mathbf{p})\, d^3p, \tag{2.7}$$

$$p = \frac{g}{(2\pi)^3} \int \frac{|\mathbf{p}|^2}{3E(\mathbf{p})}\, f(\mathbf{p})\, d^3p. \tag{2.8}$$

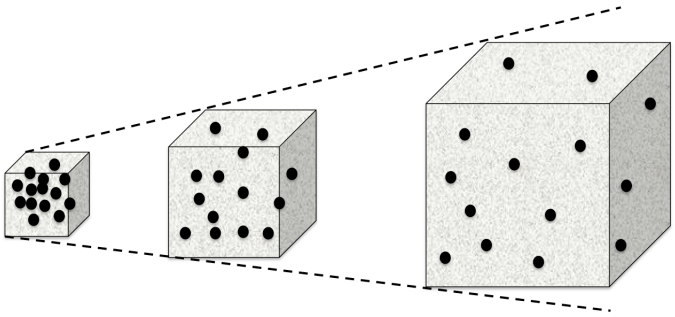

Figure 2.1 In the absence of number changing processes, the comoving number density of a species is preserved.

It is customary (and very convenient) to define densities normalised by the time dependent volume $V(t) = a(t)^3$. The reason for this is that in the absence of number changing processes, the comoving number density remains constant with time evolution (or redshift) as exemplified in Fig. 2.1. An expanding Universe is a closed system and in thermal equilibrium the total entropy is conserved.

$$TdS = d(\rho V) + pdV = d((\rho + p)V) - Vdp = 0\,, \tag{2.9}$$

where we have used that $d((\rho + p)V) = Vdp$. The entropy density is therefore $s = S/V = (\rho + p)/V$. Notice that since the evolution of the Universe is isoentropic, the entropy density $s = S/a^3$ has precisely that dependence. Applying this prescription to the number density of particles, we define the yield as a fraction of the number density and the entropy density as

$$Y = \frac{n}{s}\,. \tag{2.10}$$

Notice that, in the absence of number-changing processes, the yield remains constant. The evolution of the entropy density as a function of the temperature is given by [1]

$$s = \frac{2\pi^2}{45} g_{*s} T^3\,, \tag{2.11}$$

where the effective number of relativistic degrees of freedom for entropy is

$$g_{*s} = \sum_{\text{bosons}} g \left(\frac{T_i}{T}\right)^3 + \frac{7}{8} \sum_{\text{fermions}} g \left(\frac{T_i}{T}\right)^3\,. \tag{2.12}$$

Remember also that we can express the energy density as

$$\rho = \frac{\pi^2}{30} g_* T^4\,, \tag{2.13}$$

in terms of the relativistic number of degrees of freedom

$$g_* = \sum_{\text{bosons}} g \left(\frac{T_i}{T}\right)^4 + \frac{7}{8} \sum_{\text{fermions}} g \left(\frac{T_i}{T}\right)^4\,. \tag{2.14}$$

[1] To arrive at this equation, one can calculate $s = (p + \rho)/T$ for fermions and bosons, using the corresponding expression for the phase space distribution function.

In these two equations, T is the temperature of the plasma (in equilibrium) and T_i is the effective temperature of each species.

Solving the integral in eq. (2.6) explicitly for relativistic and non-relativistic particles, and expressing the results in terms of the Yield results in the following expressions.

- relativistic species

$$n = \frac{g_{eff}}{\pi^2}\zeta(3)T^3\,, \tag{2.15}$$

where $g_{eff} = g$ for bosons and $g_{eff} = \frac{3}{4}g$ for fermions[2]. Then, using eq. (2.10), the Yield at equilibrium reads

$$Y_{eq} = \frac{45}{2\pi^4}\zeta(3)\frac{g_{eff}}{g_{*s}} \approx 0.278\,\frac{g_{eff}}{g_{*s}}\,. \tag{2.16}$$

- non-relativistic species

$$n = g\left(\frac{mT}{2\pi}\right)^{3/2} e^{-m/T}\,. \tag{2.17}$$

Then the Yield at equilibrium reads

$$Y_{eq} = \frac{45}{2\pi^4}\left(\frac{\pi}{8}\right)^{1/2}\frac{g}{g_{*s}}\left(\frac{m}{T}\right)^{3/2} e^{-m/T}\,. \tag{2.18}$$

EXAMPLE 2.1

It is easy to estimate the value of the Yield that we need in order to reproduce the correct DM relic abundance, $\Omega h^2 \approx 0.1$, since

$$\Omega h^2 = \frac{\rho_\chi}{\rho_c}h^2 = \frac{m_\chi n_\chi h^2}{\rho_c} = \frac{m_\chi Y_\infty s_0 h^2}{\rho_c}\,, \tag{2.19}$$

where Y_∞ corresponds to the DM Yield today and s_0 is today's entropy density. We can assume that the Yield did not change since DM freeze-out and therefore

$$\Omega h^2 = \frac{m_\chi Y_f s_0 h^2}{\rho_c}\,. \tag{2.20}$$

Using the measured value $s_0 = 2970\ \text{cm}^{-3}$, and the value of the critical density $\rho_c = 1.054\times 10^{-5}\,h^2\ \text{GeV cm}^{-3}$, as well as Planck's result on the DM relic abundance, $\Omega h^2 \approx 0.1$, we arrive at

$$Y_f \approx 3.55\times 10^{-10}\left(\frac{1\ \text{GeV}}{m_\chi}\right)\,. \tag{2.21}$$

In Figure 2.2 represent the yield as a function of x for non-relativistic particles, using expression (2.18). As we can observe, the above range of viable values for Y_f correspond to $x_f \approx 20$. Notice that this is a crude approximation and we will soon be making a more careful quantitative treatment.

[2]We are using here the approximation $E \approx |\vec{\mathbf{p}}|$ in the relativistic limit, and the integrals $\int_0^\infty p^2/(e^p-1)dp = 2\zeta(3)$, and $\int_0^\infty p^2/(e^p+1)dp = 3\zeta(3)/2$, in terms or Riemann's Zeta function. Remember also that $\zeta(3) \approx 1.202$.

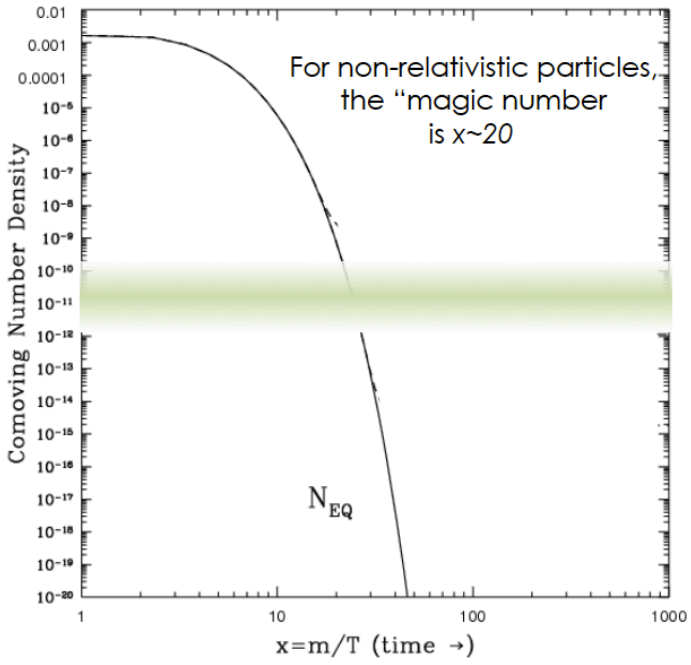

Figure 2.2 Equilibrium yield as a function of the dimensionless variable, x, for non-relativistic particles. The green band represents the freeze-out value, Y_f, for which the correct thermal relic abundance is achieved (for masses of order 1-1000 GeV.

2.2 Time evolution of the number density

The evolution of the number density operator can be computed by applying the covariant form of Liouville's operator to the corresponding phase space distribution function. Formally speaking, we have

$$\hat{L}[f] = C[f], \tag{2.22}$$

where $\hat{L}$ is the Liouville operator, defined as

$$\hat{L} = p^\mu \frac{\partial}{\partial x^\mu} - \Gamma^\mu_{\sigma\rho} p^\sigma p^\rho \frac{\partial}{\partial p^\mu}, \tag{2.23}$$

and $C[f]$ is the collisional operator, which takes into account processes which change the number of particles (e.g., annihilations or decays). In this expression, we have used the geodesic equation $dp^\mu/d\tau = d^2x^\mu/d\tau^2 = -\Gamma^\mu_{\rho\sigma}\, dx^\sigma/d\tau\, dx^\rho/d\tau = -\Gamma^\mu_{\rho\sigma} p^\sigma p^\rho$. In the expression above, gravity enters through the affine connection, $\Gamma^\mu_{\sigma\rho}$.

One can show that in the case of a FRW Universe, for which $f(x^\mu, p^\mu) = f(t, E)$, we have

$$\begin{aligned} \hat{L} &= E\frac{\partial}{\partial t} - \Gamma^0_{\sigma\rho} p^\sigma p^\rho \frac{\partial}{\partial E} \\ &= E\frac{\partial}{\partial t} - H|\mathbf{p}|^2 \frac{\partial}{\partial E}\,. \end{aligned} \tag{2.24}$$

Integrating over the phase space we can relate this to the time evolution of the number density

$$\frac{g}{(2\pi)^3}\int \frac{\hat{L}[f]}{E} d^3\mathbf{p} = \frac{g}{(2\pi)^3}\int \frac{C[f]}{E} d^3\mathbf{p}\,, \tag{2.25}$$

The integral on the left-hand side can be easily done by parts, which results in

$$\frac{dn}{dt} + 3Hn \;= \frac{g}{(2\pi)^3}\int \frac{C[f]}{E} d^3\mathbf{p}\,, \tag{2.26}$$

Regarding the collisional operator, it encodes the microphysical description in terms of Particle Physics, and incorporates all number-changing processes that create or deplete particles in the thermal bath. For simplicity, let us concentrate in annihilation processes, where SM particles $(A,\, B)$ can annihilate to form a pair of DM particles (labelled 1, 2), or vice-versa $(A,\, B \leftrightarrow 1,\, 2)$. The phase space corresponding to each particle is defined as

$$d\Pi_i = \frac{g_i}{(2\pi)^3}\,\frac{d^3\mathbf{p_i}}{2E_i}\,, \tag{2.27}$$

from where

$$\begin{aligned}
\frac{g}{(2\pi)^3}\int \frac{C[f]}{E} d^3\mathbf{p} \;&=\; -\int d\Pi_A d\Pi_B d\Pi_1 d\Pi_2 (2\pi)^4 \delta(p_A + p_B - p_1 - p_2) \\
&\quad \big[|\mathcal{M}_{12\to AB}|^2 f_1 f_2 (1 \pm f_A)(1 \pm f_B) \\
&\quad -|\mathcal{M}_{AB\to 12}|^2 f_A f_B (1 \pm f_1)(a \pm f_2)\big] \\
&=\; -\int d\Pi_A d\Pi_B d\Pi_1 d\Pi_2 (2\pi)^4 \delta(p_A + p_B - p_1 - p_2) \\
&\quad \big[|\mathcal{M}_{12\to AB}|^2 f_1 f_2 - |\mathcal{M}_{AB\to 12}|^2 f_A f_B\big]\;.
\end{aligned} \tag{2.28}$$

The terms $(1 \pm f_i)$ account for the viable phase space of the produced particles, taking into account whether they are fermions $(-)$ or bosons $(+)$. Assuming no CP violation in the DM sector (T invariance) $|\mathcal{M}_{12\to AB}|^2 = |\mathcal{M}_{AB\to 12}|^2 \equiv |\mathcal{M}|^2$. Also, energy conservation in the annihilation process allows us to write $E_A + E_B = E_1 + E_2$, thus,

$$f_A f_B = f_A^{eq} f_B^{eq} = e^{-\frac{E_A+E_B}{T}} = e^{-\frac{E_1+E_1}{T}} = f_1^{eq} f_2^{eq}\,. \tag{2.29}$$

In the first equality we have just used the fact that SM particles are in equilibrium. This eventually leads to

$$\frac{g}{(2\pi)^3}\int \frac{C[f]}{E} d^3\mathbf{p} = -\langle\sigma v\rangle \left(n^2 - n_{eq}^2\right)\,, \tag{2.30}$$

where we have defined the *thermally-averaged* cross-section as

$$\langle\sigma v\rangle \equiv \frac{1}{n_{eq}^2}\int d\Pi_A d\Pi_B d\Pi_1 d\Pi_2 (2\pi)^4 \delta(p_A + p_B - p_1 - p_2)|\mathcal{M}|^2 f_1^{eq} f_2^{eq}\,. \tag{2.31}$$

Collider enthusiasts would realise that this expression is similar to that of a cross-section, but we have to consider that the "initial conditions" do not correspond to a well-defined energy, but rather we have to integrate to the possible energies that the particles in the thermal bath may have. This explains the extra integrals in the phase space of incident

particles with a distribution function given by $f_1^{eq} f_2^{eq}$. We are thus left with the familiar form of Boltzmann equation,

$$\frac{dn}{dt} + 3Hn = -\langle \sigma v \rangle \left(n^2 - n_{eq}^2 \right) \ . \tag{2.32}$$

Notice that this is an equilibrium-restoring equation. If the right-hand-side of the equation dominates, then n traces its equilibrium value $n \approx n_{eq}$. However, when $Hn > \langle \sigma v \rangle n^2$, then the right-hand-side can be neglected and the resulting differential equation $dn/n = -3da/a$ implies that $n \propto a^{-3}$. This is equivalent to saying that DM particles do not annihilate anymore and their number density decreases only because the scale factor of the Universe increases.

It is also customary to define the dimensionless variable [3]

$$x = \frac{m}{T} \ . \tag{2.33}$$

EXAMPLE 2.2

Using the yield defined in equation (2.10) we can simplify Boltzmann equation. Notice that

$$\frac{dY}{dt} = \frac{d}{dt}\left(\frac{n}{s}\right) = \frac{d}{dt}\left(\frac{a^3 n}{a^3 s}\right) = \frac{1}{a^3 s}\left(3a^2 \dot{a} n + a^3 \frac{dn}{dt}\right) = \frac{1}{s}\left(3Hn + \frac{dn}{dt}\right). \tag{2.34}$$

Here we have used that the expansion of the Universe is iso-entropic and thus $a^3 s$ remains constant. Also we use the definition of the Hubble parameter $H = \frac{\dot{a}}{a}$. This allows us to rewrite Boltzmann equation as follows

$$\frac{dY}{dt} = -s\langle \sigma v \rangle \left(Y^2 - Y_{eq}^2 \right) \ . \tag{2.35}$$

Now, since $a \propto T^{-1}$ and $s \propto T^3$,

$$\frac{d}{dt}(a^3 s) = 0 \rightarrow \frac{d}{dt}(aT) = 0 \rightarrow \frac{d}{dt}\left(\frac{a}{x}\right) = 0 \ , \tag{2.36}$$

which in turns leads to

$$\frac{dx}{dt} = Hx \ , \tag{2.37}$$

and thus

$$\frac{dY}{dt} = \frac{dY}{dx}\frac{dx}{dt} = \frac{dY}{dx} Hx \ . \tag{2.38}$$

Using the results of Example (2.2) we can express Boltzmann equation (2.32) as

$$\begin{aligned} \frac{dY}{dx} &= \frac{-sx\langle \sigma v \rangle}{H(m)} \left(Y^2 - Y_{eq}^2 \right) \\ &= \frac{-\lambda \langle \sigma v \rangle}{x^2} \left(Y^2 - Y_{eq}^2 \right) \ , \end{aligned} \tag{2.39}$$

[3] It is important to point that this definition of x is not universal; some authors use T/m and care should be taken when comparing results from different sources in the literature.

where we have used the expression of the entropy density (2.11) in the last line and defined

$$\begin{aligned} \lambda &\equiv \frac{2\pi^2}{45}\frac{M_P\, g_{*s}}{1.66\, g_*^{1/2}} m \\ &\approx 0.26\, \frac{g_{*s}}{g_*^{1/2}} M_P\, m\,. \end{aligned} \tag{2.40}$$

Eq. (2.39) is a Riccati equation, without closed analytical form. Thus, to calculate its solutions we have to rely on numerical methods. However, it is possible to solve it approximately.

2.2.1 Freeze out of relativistic species

The freeze-out of relativistic species is easy to compute, since the yield (2.16) has no dependence on x_f . Neutrinos are a paradigmatic example of relativistic particles and one must in principle consider their contribution to the total amount of dark matter (after all, they are dark).

Since neutrinos decouple while they are still relativistic, their yield reads

$$Y_{eq} \approx 0.278\, \frac{g_{eff}}{g_{*s}}\,. \tag{2.41}$$

Neutrinos decouple at a few MeV, when the species that were still relativistic are $e^{\pm}$, γ, ν and $\bar{\nu}$. Thus, the number of relativistic degrees of freedom is $g_* = g_{*s} = 10.75$. For one neutrino family, the effective number of degrees of freedom is $g_{eff} = 3g/4 = 3/2$. Using these values, the relic density today an be written as

$$\begin{aligned} \Omega h^2 &= \frac{\sum_i m_{\nu_i} Y_\infty s_0 h^2}{\rho_c} \\ &\approx \frac{\sum_i m_{\nu_i}}{91\,\mathrm{eV}}\,. \end{aligned} \tag{2.42}$$

Notice that in order for neutrinos to be the bulk of dark matter, we would need $\sum_i m_{\nu_i} \approx 9\,\mathrm{eV}$, which is much bigger than current upper limits (for example, obtained from cosmological observations). Notice, indeed, that if we consider the current bound $\sum_i m_{\nu_i} \leq 0.3\,\mathrm{eV}$ we can quantify the contribution of neutrinos to the total amount of dark matter, resulting in $\Omega h^2 \leq 0.003$. This is less than a 3% of the total dark matter density.

2.2.2 Freeze out of non-relativistic species

The case of non-relativistic species is far more interesting. Once We can define the quantity

$$\Delta_Y \equiv Y - Y_{eq}\,. \tag{2.43}$$

Boltzmann equation (2.39) is now easier to solve, at least approximately, as follows

- For early times, $1 < x \ll x_f$, the yield follows closely its equilibrium value, $Y \approx Y_{eq}$, and we can assume that $d\Delta_Y/dx = 0$. We then find

$$\Delta_Y = -\frac{\frac{dY_{eq}}{dx}}{Y_{eq}}\,\frac{x^2}{2\lambda\langle\sigma v\rangle}\,. \tag{2.44}$$

Thus, at freeze-out we obtain

$$\Delta_{Y_f} \approx \frac{x_f^2}{2\lambda\langle\sigma v\rangle} , \tag{2.45}$$

where in the last line we have used that for large enough x, using eq. (2.18) implies $\frac{dY_{eq}}{dx} \approx -Y_{eq}$.

- For late times, $x \gg x_f$, we can assume that $Y \gg Y_{eq}$, and thus $\Delta_{Y_\infty} \approx Y_\infty$, leading to the following expression,

$$\frac{d\Delta_Y}{dx} \approx -\frac{\lambda\langle\sigma v\rangle}{x^2}\Delta_Y^2 , \tag{2.46}$$

This is a separable equation that we integrate from the freeze-out time up to nowadays. In doing so, it is customary to expand the thermally averaged annihilation cross section in powers of x^{-1} as $\langle\sigma v\rangle = a + \frac{b}{x}$.

$$\int_{\Delta_{Y_f}}^{\Delta_{Y\infty}} \frac{d\Delta_Y}{\Delta_Y^2} = -\int_{x_f}^{x_\infty} \frac{\lambda\langle\sigma v\rangle}{x^2} dx . \tag{2.47}$$

Taking into account that $x_\infty \gg x_f$, this leads to

$$\frac{1}{\Delta_{Y_\infty}} = \frac{1}{\Delta_{Y_f}} + \frac{\lambda}{x_f}\left(a + \frac{b}{2x_f}\right) . \tag{2.48}$$

The term $1/\Delta_{Y_f}$ is generally ignored (if we are only aiming at a precision up to a few per cent [18]) . We can check that this is a good approximation using the previously derived (2.45) for $x_f \approx 20$ (which, as we saw in Fig. 2.2 is the value for which the equilibrium Yield has the right value). This leads to

$$\Delta_{Y_\infty} = Y_\infty = \frac{x_f}{\lambda\left(a + \frac{b}{2x_f}\right)} . \tag{2.49}$$

The relic density can now be expressed in terms of this result as follows

$$\begin{aligned} \Omega h^2 &= \frac{m_\chi\, Y_\infty\, s_0 h^2}{\rho_c} \\ &\approx \frac{10^{-10}\ \mathrm{GeV}^{-2}}{a + \frac{b}{40}} \\ &\approx \frac{3\times 10^{-27}\ \mathrm{cm}^3\, s^{-1}}{a + \frac{b}{40}} . \end{aligned} \tag{2.50}$$

This expression explicitly shows that for larger values of the annihilation cross section, smaller values of the relic density are obtained.

2.2.3 WIMPs

Equation (2.50) implies that in order to reproduce the correct relic abundance, dark matter particles must have a thermally averaged annihilation cross section (from now on we will

shorten this to simply annihilation cross section when referring to $\langle\sigma v\rangle$) of the order of $\langle\sigma v\rangle \approx 3 \times 10^{-26}$ cm^3 s^{-1}.

We can now consider a simple case in which dark matter particles self-annihilate into Standard Model ones through the exchange (e.g., in an s-channel) of a gauge boson. It is easy to see that if the annihilation cross section is of order $\langle\sigma v\rangle \sim G_F^2 m_{WIMP}^2$, where $G_F = 1.16 \times 10^{-5}$ GeV^{-2}, then the correct relic density is obtained for masses of the order of $\sim$ GeV.

2.3 Computing the DM annihilation cross section

In the previous sections we have derived a relation between the thermally averaged annihilation cross section and the corresponding dark matter relic abundance. This is very useful, since it provides an explicit link with particle physics. A central point in that calculation was the expansion in velocities of the thermally averaged annihilation cross section.

$$\langle\sigma v\rangle = \langle a + bv^2 + cv^4 + \ldots\rangle = a + \frac{3}{2}\frac{b'}{x} + \frac{15}{8}\frac{c}{x^2} + \ldots \,. \tag{2.51}$$

Notice that in the expressions of the previous section we have defined $b \equiv 3b'/2$. As we also mentioned before, DM candidates tend to decouple when $x_f \approx 20$. For this value, the rms velocity of the particles is about c/4, thus corrections of order x^{-1} can in general not be ignored (they can be of order $5 - 10\%$). Moreover, some selection rules can actually lead to $a = 0$ for some particular annihilation channels and in that case $\langle\sigma v\rangle$ is purely velocity-dependent.

It is important to define correctly the relative velocity that enters the above equation. In Ref. [18] an explicitly Lorentz-invariant formalism is introduced where

$$g_1 \int C[f_1]\frac{d^3p_1}{2\pi^3 E_1} = -\int \langle\sigma v\rangle_{\rm M\o l}(dn_1 dn2 - dn_1^{eq} dn_2^{eq}) \,, \tag{2.52}$$

where $\langle\sigma v\rangle_{\rm M\o l} n_1 n_2$ is invariant under Lorentz transformations and equals $v_{lab} n_{1,lab} n_{2,lab}$ in the rest frame of one of the incoming particles. In our case the densities and Møller velocity refer to the cosmic comoving frame. In terms of the particle velocities $\vec{v}_i = \vec{p}_i/E_i$,

$$v_{\rm M\o l} = \left[|\vec{v}_1 - \vec{v}_2|^2 + |\vec{v}_1 \times \vec{v}_2|^2\right]^{1/2} \,. \tag{2.53}$$

The thermally-averaged product of the dark matter pair-annihilation cross section and their relative velocity $\langle\sigma v_{\rm M\o l}\rangle$ is most properly defined in terms of separate thermal baths for both annihilating particles [18, 19],

$$\langle\sigma v_{\rm M\o l}\rangle(T) = \frac{\int d^3p_1 d^3p_2 \, E\sigma v_{\rm M\o l} \, e^{-E_1/T} e^{-E_2/T}}{\int d^3p_1 d^3p_2 E e^{-E_1/T} e^{-E_2/T}} \,, \tag{2.54}$$

where $p_1 = (E_1, \mathbf{p_1})$ and $p_2 = (E_2, \mathbf{p_2})$ are the 4-momenta of the two colliding particles, and T is the temperature of the bath. The above expression can be reduced to a one-dimensional integral which can be written in a Lorentz-invariant form as [18]

$$\langle\sigma v_{\rm M\o l}\rangle(T) = \frac{1}{8m_\chi^4 T K_2^2(m_\chi/T)} \int_{4m_\chi^2}^{\infty} ds \, \sigma(s)(s - 4m_\chi^2)\sqrt{s} K_1\left(\frac{\sqrt{s}}{T}\right) \,, \tag{2.55}$$

where $s = (p_1 + p_2)^2$ and K_i denote the modified Bessel function of order i. In computing the relic abundance [20] one first evaluates eq. (2.55) and then uses this to solve the Boltzmann equation. The freeze out temperature can be computed by solving iteratively the equation

$$x_f = \ln\left(\frac{m_\chi}{2\pi^3}\sqrt{\frac{45}{2g_* G_N}}\,\langle\sigma v_{\rm M\o l}\rangle(x_f)\,x_f^{-1/2}\right) \tag{2.56}$$

where g_* represents the effective number of degrees of freedom at freeze-out ($\sqrt{g_*} \approx 9$). As explained in the previous section, one finds that the freeze-out point $x_f \equiv m_\chi/T_f$ is approximately $x_f \sim 20$.

The procedure can be simplified if we consider that the annihilation cross section can be expanded in plane waves. For example, consider the dark matter annihilation process $\chi\chi \to ij$ and assume that the thermally averaged annihilation cross section can be expressed as $\langle\sigma v\rangle_{ij} \approx a_{ij} + b_{ij}x$. It can then be shown that the coefficients a_{ij} and b_{ij} can be computed from the corresponding matrix element. For example,

$$a_{ij} = \frac{1}{m_\chi^2}\left(\frac{N_c}{32\pi}\beta(s, m_i, m_j)\frac{1}{2}\int_{-1}^{1} d\,\cos\theta_{CM}|\mathcal{M}_{\chi\chi\to ij}|^2\right)_{s=4m_\chi^2}, \tag{2.57}$$

where θ_{CM} denotes the scattering angle in the CM frame, $Nc = 3$ for $\bar{q}q$ final states and 1 otherwise, and

$$\beta(s, m_i, m_j) = \left(1 - \frac{(m_i + m_j)^2}{s}\right)^{1/2}\left(1 - \frac{(m_i - m_j)^2}{s}\right)^{1/2} \tag{2.58}$$

The contribution for each final state is calculated separately.

2.3.1 Special cases

The derivation of equation (2.50) relied on the expansion of $\langle\sigma v\rangle$ in terms of plane waves. This expansion can be done when $\langle\sigma v\rangle$ varies slowly with the energy (we can express this in terms of the centre of mass energy s). However, there are some special cases in which this does not happen and which deserve further attention.

- Annihilation thresholds

  A new annihilation channel $\chi + \chi \to A + B$ opens up when $2m_\chi \approx m_A + m_B$. In this case the expansion in velocities of $\langle\sigma v\rangle$ diverges (at the threshold energy) and it is no longer a good approximation [18]. Notice in particular that below the threshold, the expression of a_{ij} in Equation (2.57) is equal to zero (as it is only evaluated for $s > 4m_\chi^2$). A qualitative way of understanding this is of course that DM particles have a small velocity, which is here approximated to zero. In the limit of zero velocity, the total energy available is determined by the DM mass.

  However, we are here ignoring that a fraction of DM particles (given by their thermal distribution in the Early Universe) have a kinetic energy sufficient to annihilate into heavier particles (above the threshold). In other words, $\langle\sigma v\rangle$ is different from zero below the corresponding thresholds. A very good illustration of this effect is shown in Ref. [18] and is here reproduced in Fig. 2.3.

  The thin solid line corresponds to the approximate expansion in velocities and shows that not only $\langle\sigma v\rangle$ is zero below the threshold, but also diverges at the threshold,

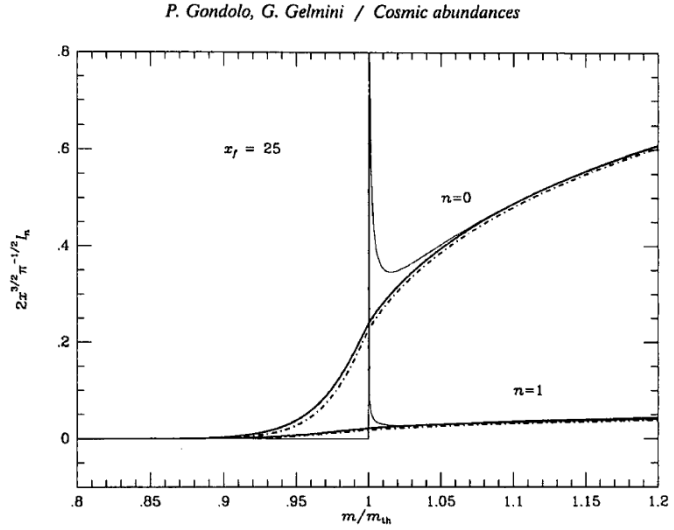

Figure 2.3 Relativistic thermal average near a threshold (thick solid line) compared to the result fro the expansion in powers of x^{-1} (thin line). Figure from Ref. [18].

thereby not leading to a good solution. Expression (2.55), represented by a thick solid line, still provides a good solution .

- Resonances

  The annihilation cross section is not a smooth function of s in the vicinity of an s-channel resonance. Thus, the velocity expansion of $\langle\sigma v\rangle$ will fail (although once more, expression (2.55) still provides a good solution). For a Breit-Wigner resonance (due to a particle ϕ) we have

$$\sigma = \frac{4\pi w}{p^2} B_i B_f \frac{m_\phi^2 \Gamma_\phi^2}{(s-m_\phi^2)^2 + m_\phi^2 \Gamma_\phi^2} \,, \tag{2.59}$$

  in terms of the centre of mass momentum $p = 1/2(s-4m^2)^{1/2}$ and the statistical factor $w = (2J+1)/(2S+1)^2$. The quantities $B_{i,f}$ correspond to the branching fractions of the resonance into the initial and final channel.

  We can define the kinetic energy per unit mass in the lab frame, ϵ, as

$$\epsilon = \frac{(E_{1,lab}-m)+(E_{2,lab}-m)}{2m} = \frac{2-4m^2}{4m^2} \,, \tag{2.60}$$

  and rewrite the expression for σ in the lab frame (we want to use Equation (3.21) in Ref. [18] to compute $\langle\sigma v_{\rm M\o l}\rangle$). Summing to all final states, and using $v_{lab} = 2\epsilon^{1/2}(1+\epsilon)^{1/2}/(1+2\epsilon)$, we obtain

$$\sigma v_{lab} = \frac{8\pi w}{m^2} b_\phi(\epsilon) \frac{\gamma_\phi^2}{(\epsilon-\epsilon_\phi^2)^2 + \gamma_\phi^2} \,, \tag{2.61}$$

  with the definitions $b(\epsilon) = B_i(1-B_i)(1+\epsilon)^{1/2}/(\epsilon^{1/2}(1+2\epsilon)$, $\gamma_\phi = m_\phi\Gamma_\phi/4m^2$, and $\epsilon_\phi = (m_\phi^2 - 4m^2)/4m^2$.

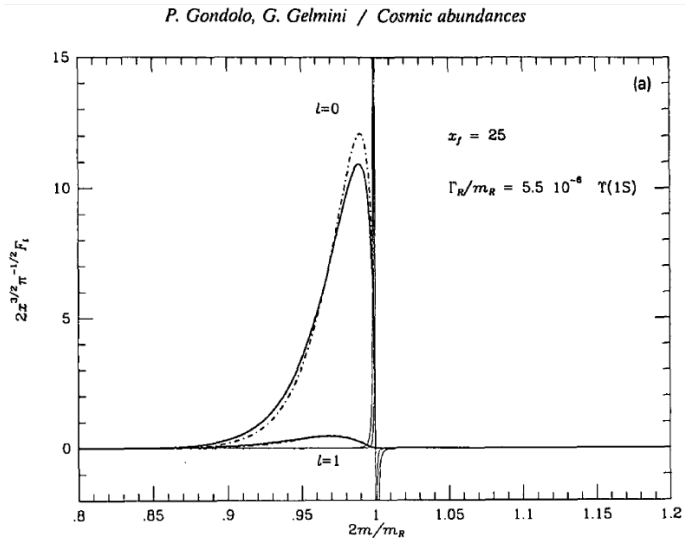

Figure 2.4 Relativistic thermal average in a resonance (thick solid line) compared to the result fro the expansion in powers of x^{-1} (thin line). Figure from Ref. [18].

It can be shown that in the case of a very narrow resonance, $\gamma_\phi \ll 1$, the expression above can be approximated as

$$\sigma v_{lab} = \frac{8\pi w}{m^2} b_\phi(\epsilon)\pi\gamma_\phi\delta(\epsilon - \epsilon_\phi) \,, \tag{2.62}$$

the relativistic formula for the thermal average then reads [18]

$$\langle\sigma v_{\text{Møl}}\rangle = \frac{16\pi w}{m^2}\frac{x}{K_2^2(x)}\pi\gamma_\phi\epsilon_\phi^{1/2}(1+2e_\phi)K_1(2x\sqrt{1+\epsilon_\phi})b_\phi(e_\phi)\theta(\epsilon_\phi) \,. \tag{2.63}$$

Notice that $\epsilon_\phi > 0$ when $m < 2m_\phi$, i.e., when the mass of the DM is not enough to enter the resonance. The reason is easy to understand. Only through the extra kinetic energy provided by the thermal bath, the resonance condition can be satisfied. However, when the mass of the DM exceeds the resonance condition, the kinetic energy only takes us further away from the resonant condition and the thermalised cross section tends to vanish. In other words, the centre of mass rest energy exceeds $m_\phi/2$. This can be seen in Figure 2.4.

For a large width the expression has to be computed numerically and can be found in Ref. [18].

- Coannihilations

When deriving Boltzmann equation (2.32) we have only considered one exotic species, but this needs not be the case. In fact, in most particle models for DM, there are more exotic species that we need to take into account. Notice that, in principle, this would lead to a system of coupled Boltzmann equations. If we label exotic species as χ_i, with $i = 0,\ 1 \ldots k$, and SM particles as $A,\ B$, we have to consider all number chang-

ing processes for each species,

$$\begin{aligned} (i) \quad & \chi_i + \chi_j \to A + B \\ (ii) \quad & \chi_i + A \to \chi_j + B \\ (iii) \quad & \chi_j \to \chi_i + A \end{aligned}$$

If we consider the (usual) case in which the DM is protected by a symmetry (e.g., in the case of Supersymmetric theories) and that the exotic particles all must decay eventually into the lightest one χ_0, then, we must only trace the evolution of the total number density of exotic species, $n = \sum_{i=0}^{k} n_i$. Under this assumption, processes (ii) and (iii) do not need to be considered, as they do not change the number of exotics. This is correct as long as the rate of these is faster than the expansion of the Universe.

Regarding process (i) we have to be aware that the cross section σ_{ij} is going to appear multiplied by the corresponding number densities, $n_i n_j$. Now, we are considering the case in which both particles i and j are non-relativistic and as a consequence, $n_{i,j}$ are Boltzmann suppressed, $n_{i,j}/e^{-m_{i,j}/T}$. Thus, unless $m_j \approx m_i$, the abundance of χ_j is negligible and only the process $\chi_i + \chi_j \to A + B$ is important (and we are back to the case of a single exotic).

However, when $m_j \approx m_i$, there can be coannihilation effects and particle j may serve as a channel through which particles i can be more effectively depleted. This is the case, e.g., of the stau and the neutralino in supersymmetric theories.

2.4 Freeze-in of dark matter

In the previous section, we have explained in full detail how DM particles can be produced in the early Universe through pair-annihilation processes. As we discussed earlier, if the annihilation cross section happens to be of the order to the Electroweak scale, the resulting relic density is of the right order to reproduce the observed DM abundance. However, this WIMP paradigm is by no means the only way in which DM particles can be produced in the right amount. In this section, we will address another interesting possibility that is applicable to particles with a much smaller interaction scale.

Let us begin by assuming that the DM particles, χ, has extremely weak interactions, and that its initial abundance is zero. An implicit assumption in all of this is that the reheating temperature of the Universe after inflation was not high enough for χ to be in thermal equilibrium. Notice that DM particles can still be produced by interactions of particles in the thermal bath (following the notation of Ref. [21], we will refer to bath particles as B_i). The production rate is small, as a consequence of the small DM coupling, however, since they are produced out of equilibrium, these DM particles do not annihilate (and of course do not decay). As a consequence, a relic density builds up. The final DM density depends on the specific interactions with bath particles.

In order to carry out the computation, notice that we can make use of Boltzmann equation, as formulated in eq. (2.26), but now we have to write the collisional operator according to the interactions of DM particles with those of the bath. We will here consider one characteristic example, that should serve as a guide to consider other possibilities.

2.4.1 DM production from decays of heavier bath particles

Consider the decay of a heavy bath particle into a lighter one and a DM particle, $B_2 \to B_1\chi$. If $m_{B2} > m_{B1} + m_\chi$ this process will dominate DM production. The collisional operator is easy to write,

$$\begin{aligned}\frac{dn}{dt} + 3Hn &= \frac{g}{(2\pi)^3}\int \frac{C[f]}{E} d^3\mathbf{p} \\ &= \int d\Pi_{B_1} d\Pi_{B_2} d\Pi_\chi \, (2\pi)^4 \delta^4 \left(p_{B_2} - p_{B_1} - p_\chi\right) \times \\ &\quad \left[\left|\mathcal{M}_{B_2 \to B_1\chi}\right|^2 f_{B_2}(1 \pm f_{B_1})(1 \pm f_\chi) - \left|\mathcal{M}_{B_1\chi \to B_2}\right|^2 f_{B_1} f_\chi (1 \pm f_{B_2}) \right] \\ &= \int d\Pi_{B2} \Gamma_{B2} 2 g_{B2} m_{B2} f_{B2} \, . \end{aligned} \tag{2.64}$$

In the last line we have assumed no Pauli blocking to approximate $(1 \pm f_{B_1}) \approx 1$ and we have neglected the initial abundance of DM particles, $f_\chi \approx 0$. We have also expressed $\left|\mathcal{M}_{B_2 \to B_1\chi}\right|^2$ in terms of the decay width, Γ_{B2}, the number of degrees of freedom ob B_2 and its mass. If we write the phase space element explicitly, and we consider that for particles in thermal equilibrium we can approximate $f_{B_2} = 1/(e^{E_{B_2}/T} \pm 1) \approx e^{-E_{B_2}/T}$, we are left with

$$\frac{dn}{dt} + 3Hn = g_{B_2} \int_{m_{B_2}}^{\infty} \frac{d^3 p_{B_2}}{(2\pi)^3} \frac{f_{B_2} \Gamma_{B_2} m_{B_2}}{E_{B_2}} \, . \tag{2.65}$$

The integral on the right-hand side is easy to solve, as it can be reduced to the first modified Bessel function of the second kind, $K_1(m_{B_2}/T)$, resulting in

$$\frac{dn}{dt} + 3Hn = \frac{g_{B_2} \Gamma_{B_2} m_{B_2}^2}{2\pi^2} \, T \, K_1(m_{B_2}/T) \, . \tag{2.66}$$

As we did in the previous section, it is much simpler to rewrite this expression in terms of the derivative of the yield $Y = n/s$ in terms of the dimensionless variable $x = m_{B_2}/T$, which leads to

$$Y = \frac{45 g_{B_2} M_p \Gamma_{B_2}}{4\pi^4 (1.66) m_{B_2}^2 g_*^S \sqrt{g_*}} \int_{x_{min}}^{\infty} K_1(x) \, x^3 \, dx \, . \tag{2.67}$$

Finally, solving for $x_{min} = 0$, yields

$$Y \approx \frac{135 \, g_{B_2}}{8\pi^3 (1.66) g_*^S \sqrt{g_*}} \left(\frac{\Gamma_{B2} M_p}{m_{B_2}^2} \right) \, . \tag{2.68}$$

The function $K_1(x) \, x^3$ has a maximum around $x \approx 2.4$ and its integral $\int_0^{x_{max}} K_1(x) \, x^3 dx$ stabilises above $x_{max} \approx 8$, we have plotted this behaviour in Fig. 2.5. As we can observe, the final yield is proportional to the bath's particle partial decay width. This is very interesting, as the decay width is directly proportional to the DM coupling square. Thus, the final yield (and DM relic abundance) increases if the DM coupling increases. This behaviour is the opposite as observed for WIMPs in eq.(2.49). This behaviour holds as long as the DM coupling is small. If we increase the DM coupling, there comes a point at which the DM particles produced reach thermal equilibrium and then we have to go back to the freeze-out computation of the previous section.

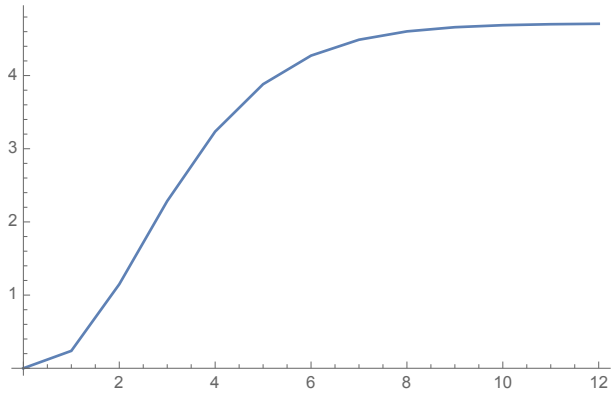

Figure 2.5 Yield of a freeze-in species (in arbitrary units) as a function of $x = m/T$.

Finally, from eq.(2.68) we can use the explicit expression for the partial decay width in a two-body final state and compute the resulting relic density. It can be seen that in order to reproduce the correct relic abundance, the coupling needed is of the order of $\lambda \approx 10^{-13}$. Interestingly, the final value of the Yield is also sensitive to the initial value of x_{min} from which we integrate. Notice that x_{min} will be given by the temperature at which the Universe reheated after inflation. Thus, the frreeze-in mechanism has a very interesting connection to inflation.

A similar computation can be made for other possible production channels, for example, scattering of bath particles $B_1 B_2 \to B_3 \chi$. In this case, the Boltzmann equation (2.64) has to be modified accordingly taking into account the matrix elements of the process and the number densities of the particles involved.

The freeze in mechanism has been used for example to argue that gravitinos (the supersymmetric companion of the graviton) and axinos (the supersymmetric companion of the axion) can be viable candidates for DM.

2.5 Late decays of unstable particles

As we have just seen in the freeze-in mechanism of the previous section, it is conceivable that particles with a small coupling to SM ones are produced out of equilibrium due to either scattering or decays of particles in the thermal bath. The frozen-in particles need not be absolutely stable, but given their small couplings their lifetime can be large. If the lifetime is larger than the age of the Universe (10^{17} s), we should not worry as the computation of the relic density is not altered and this simply corresponds to a case of decaying DM (very interesting from the point of view of indirect detection). However, if the lifetime is smaller, then it is obvious that this particle cannot be the DM. Late-decaying particles can however contribute to the (non-thermal) production of DM. A possible scenario is as follows.

Consider a canonical WIMP DM candidate, χ_1, which decoupled at $x = m_{\chi_1}/T \approx 20$ via a freeze-out mechanism as described in Section 2.2.2, which leads to to a *thermal* relic abundance $Y^{th}_{\chi_1}$. Simultaneously, a semi-stable particle χ_2, with very small couplings, freezes-in via the mechanism explained in Section 2.4, with a yield Y_{χ_2}. If particle χ_2

can decay into particle χ_1 (after the latter has frozen-out), then eventually all the number density of the heavy particle, is translated into the lighter one leading to a *non-thermal* contribution, $Y_{\chi_2} = Y^{nt}_{\chi_1}$. The total yield for the lighter particle is therefore the sum of both contributions

$$Y_{\chi_1} = Y^{th}_{\chi_1} + Y^{nt}_{\chi_1}. \tag{2.69}$$

This exotic scenario can occur in supersymmetric models, where χ_2 is the gravitino and χ_1 is the lightest neutralino. It should be emphasized that the late decay of exotic particles (and the associated injection of electromagnetic and hadronic particles) can ruin the predictions of BBN and also alter the black body shape of the CMB spectrum. Stringent constraints exist if these decays occur after BBN, but in general the model is safe if the lifetime of χ_2 is smaller than approximately 1 minute.

CHAPTER 3

DIRECT DM DETECTION

3.1 Preliminaries

3.1.1 DM flux

We can easily estimate the flux of DM particles through the Earth. The DM typical velocity is of the order of $300\,\mathrm{km\,s^{-1}} \sim 10^{-3}\,c$. Also, the local DM density is $\rho_0 = 0.3\,\mathrm{GeV\,cm^{-3}}$, thus, the DM number density is $n = \rho/m$.

$$\phi = \frac{v\rho}{m} \approx \frac{10^7}{m}\,\mathrm{cm^{-2}\,s^{-1}} \tag{3.1}$$

These particles interact very weakly with SM particles.

Assuming a typical WIMP cross section σ

3.1.2 Kinematics

Direct DM detection is based on the search of the scattering between DM particles and nuclei in a detector. This process is obly observable through the recoiling nucleus, with an energy E_R. DM particles move at non-relativistic speeds in the DM halo. Thus, the dynamics of their elastic scattering off nuclei are easily calculated. In particular, the recoiling energy of the nucleus is given by

$$E_R = \frac{1}{2} m_\chi\, v^2\, \frac{4 m_\chi m_N}{(m_\chi + m_N)^2}\, \frac{1+\cos\theta}{2} \tag{3.2}$$

It can be checked that for DM particles with a mass of the order of 100 GeV, this leads to recoil energies of approximately $E_R \sim 100$ keV. Notice also that the maximal energy transfer occurs on a head-on-collision and when the DM mass is equal to the target mass. In such a case

$$E_R^{max} = \frac{1}{2} m_\chi \, v^2 = \frac{1}{2} m_\chi \times 10^{-6} = \frac{1}{2} \left(\frac{m_\chi}{1\,\mathrm{GeV}} \right) \,\mathrm{keV} \tag{3.3}$$

where we have used that in a DM halo the typical velocity is $v \sim 10^{-3} c$.

Experiments must therefore be very sensitive and be able to remove an overwhelming background of ordinary processes which lead to nuclear recoils of the same energies.

3.2 The master formula for direct DM detection

The total number of detected DM particles, N, can be understood as the product of the DM flux (which is equal to the DM number density, n, times its speed, v), times the effective area of the target (i.e., the number of targets N_T times the scattering cross-section, σ), all of this multiplied by the observation time, t,

$$N = t \, n \, v \, N_T \, \sigma \, . \tag{3.4}$$

We will be interested in determining the spectrum of DM recoils, i.e., the energy dependence of the number of detected DM particles. Thus,

$$\frac{dN}{dE_R} = t \, n \, v \, N_T \, \frac{d\sigma}{dE_R} \, . \tag{3.5}$$

Now, the DM velocity is not unique, and in fact DM particles are described by a local velocity distribution, $f(\vec{v})$, where $\vec{v}$ is the DM velocity in the reference frame of the detector. We therefore have to integrate to all possible DM velocities, with their corresponding probability density,

$$\frac{dN}{dE_R} = t \, n \, N_T \int_{v_{min}} v f(\vec{v}) \, \frac{d\sigma}{dE_R} \, d\vec{v} \, , \tag{3.6}$$

where

$$v_{min} = \sqrt{m_\chi \, E_R / 2\mu_{\chi N}^2} \tag{3.7}$$

is the minimum speed necessary to produce a DM recoil of energy E_R, in terms of the WIMP-nucleus reduced mass, $\mu_{\chi N}$. Using $n = \rho / m_\chi$ and $N_T = M_T / m_N$ (where M_T is the total detector mass and m_N is the mass of the target nuclei), and defining the experimental exposure $\epsilon = t \, M_T$, we arrive at the usual expression for the DM detection rate

$$\frac{dN}{dE_R} = \epsilon \, \frac{\rho}{m_\chi \, m_N} \int_{v_{min}} v f(\vec{v}) \, \frac{d\sigma}{dE_R} \, d\vec{v} \, . \tag{3.8}$$

3.2.1 The scattering cross section

The scattering takes place in the non-relativistic limit. The cross section is therefore approximately isotropic (angular terms being suppressed by $v^2/c^2 \sim 10^{-6}$. This implies that

$$\frac{d\sigma}{d\cos\theta^*} = \text{constant} = \frac{\sigma}{2} \tag{3.9}$$

On the other hand,

$$E_R = E_R^{max}\,\frac{1+\cos\theta^*}{2} \quad \rightarrow \quad \frac{dE_R}{d\cos\theta^*} = \frac{E_R^{max}}{2} \tag{3.10}$$

From this, we can see that

$$\frac{d\sigma}{dE_R} = \frac{d\sigma}{d\cos\theta^*}\frac{d\cos\theta^*}{dE_R} = \frac{\sigma}{E_R^{max}} = \frac{m_N}{2\mu_{\chi N}^2}\frac{\sigma}{v^2} \tag{3.11}$$

Notice finally that the momentum transfer from WIMP interactions reads (remember that we are considering non-relativistic processes and thus we neglect the kinetic energy of the nucleus)

$$q = \sqrt{2\,m_N\,E_R} \tag{3.12}$$

and is typically of the order of the MeV. The equivalent de Broglie length would be $\lambda \sim 2\pi\hbar/p \sim 10 - 100$ fm. For light nuclei, the DM particle sees the nucleus as a whole, without substructure, only for heavier nuclei we have to take into account a suppression form factor. The nuclear form factor, $F^2(E_R)$, accounts for the loss of coherence

$$\frac{d\sigma}{dE_R} = \frac{m_N}{2\mu_{\chi N}^2}\frac{\sigma_0}{v^2}\,F^2(E_R) \tag{3.13}$$

Finally, the scattering cross section receives different contributions, depending on the microscopic description of the interaction.

In the end, we can

$$\frac{dN}{dE_R} = \epsilon\,\frac{\rho}{2\,m_\chi\,\mu_{\chi N}^2}\,\sigma_0\,F^2(E_R)\int_{v_{min}}\frac{f(\vec{v})}{v}\,d\vec{v}\,. \tag{3.14}$$

The inverse mean velocity

$$\eta(v_{min}) = \int_{v_{min}}\frac{f(\vec{v})}{v}\,d\vec{v}\,. \tag{3.15}$$

is the main Astrophysical input.

3.2.2 The importance of the threshold

From the kinematics of the DM-nucleus interaction, we see that, for a given recoil energy E_R, we require a minimal velocity of DM particles, given by expression (3.7).

Thus, given that experiments are only sensitive to DM interactions above a certain energy threshold, E_T, this means that we are only probing a part of the WIMP velocity distribution function (for a given DM mass). Conversely, given that DM particles have a maximum velocity in the halo (otherwise they become unbound and escape the galaxy), the experimental energy threshold is a limitation to explore low-mass WIMPs.

EXAMPLE 3.1

Consider a germanium experiment and a xenon experiment with a threshold of 2 keV. Given the escape velocity in a canonical isothermal halo, $v_{esc} = 554\ \mathrm{km\,s^{-1}}$, determine the minimum DM mass that these experiments can probe.

This is the reason that experiments loose sensitivity for small masses.

3.2.3 Velocity distribution function

It is customary to consider the Isothermal Spherical Halo, which assumes that the Milky Way (MW) halo is an isotropic, isothermal sphere with density profile $\rho \propto r^{-2}$. The velocity distribution, in the galactic rest frame, for such a halo reads

$$f_{gal}(\vec{v}) = \frac{1}{(2\pi\sigma)^{3/2}} e^{-\frac{|\vec{v}|^2}{2\sigma^2}}, \tag{3.16}$$

where the one-dimensional velocity dispersion, σ, is related to the circular speed, v_c, as $\sigma = v_c/\sqrt{2}$. The canonical values are $v_c = 220\text{km}\,\text{s}^{-1}$, with a statistical error of order 10% (see references in [22])

Now, in order to use it for direct detection experiments we need to carry out a Galilean transformation $\vec{v} \to \vec{v} + \vec{v}_E$, such that

$$f(\vec{v}) = f_{gal}(\vec{v} + \vec{v}_E(t)). \tag{3.17}$$

where $\vec{v}_E(t)$ is the velocity of the Earth with respect to the Galactocentric rest frame.

$$\vec{v}_E(t) = \vec{v}_{LRF} + \vec{v}_{\odot} + \vec{v}_{orbit}(t) \tag{3.18}$$

Notice that v_E includes contributions from the speed of the Local Standard of Rest v_{LSR}, the peculiar velocity of the Sun with respect to v_{LSR}, and the Earth's velocity around the Sun, which has an explicit time dependence.

Notice that if we work with the SHM, the angular integration in the computation of direct detection rates can be easily done as follows

$$\begin{aligned}
\int \frac{f(\vec{v})}{v} d^3v &= \int d\phi \int d\cos\theta \int dv\, v \frac{1}{(2\pi\sigma^2)^{3/2}} e^{-\frac{|\vec{v}|^2+|\vec{v}_E|^2}{2\sigma^2}} e^{\frac{|\vec{v}|\,|\vec{v}_E|\cos\theta}{\sigma^2}} \\
&= 2\pi \int dv\, v \frac{2\sigma^2}{|v||\vec{v}_E|(2\pi\sigma)^{3/2}} e^{-\frac{|\vec{v}|^2+|\vec{v}_E|^2}{2\sigma^2}} \sinh\left(\frac{|\vec{v}|\,|\vec{v}_E|}{\sigma^2}\right) \\
&= \int dv\, \frac{\sqrt{2}}{\sqrt{\pi}\sigma|\vec{v}_E|}\, e^{-\frac{|\vec{v}|^2+|\vec{v}_E|^2}{2\sigma^2}} \sinh\left(\frac{|\vec{v}|\,|\vec{v}_E|}{\sigma^2}\right)
\end{aligned} \tag{3.19}$$

3.2.4 Energy resolution, threshold energy and experimental efficiency

3.3 Exponential spectrum

$$\eta(v_{min}) \propto e^{-\alpha E_R} \tag{3.20}$$

3.4 Annual modulation

$$v_E(t) = v_0\,[1.05 + 0.07\cos(2\pi(t - t_p)/1\text{yr})] \tag{3.21}$$

The amplitude of the modulation in the velocity is very small, approximately a 7% ($v_{orbit}\cos\theta_{orbit}/(v_{LRF} + v_{\odot}) \approx 15/220$

This eventually implies a modulation in $\eta(v_{min})$, which means that the amount of DM particles in the tail of the distribution can change substantially. This, in turn, leads to a modulation in the detected rate.

3.5 Directional detection

The current experimental situation regarding directional DM detection has been summarised in the recent review article, Ref. [22].

3.6 Coherent neutrino scattering

Solar neutrinos might leave a signal in DD experiments, either through their coherent scattering with the target nuclei or through scattering with the atomic electrons.

In general, the number of recoils per unit energy can be written

$$\frac{dR}{dE_R} = \frac{\epsilon}{m_T} \int dE_\nu \frac{d\phi_\nu}{dE_\nu} \frac{d\sigma_\nu}{dE_R}, \tag{3.22}$$

where ϵ is the exposure and m_T is the mass of the target electron or nucleus. If several isotopes are present, a weighted average must be performed over their respective abundances.

The SM neutrino-electron scattering cross section is

$$\begin{aligned} \frac{d\sigma_{\nu e}}{dE_R} &= \frac{G_F^2 m_e}{2\pi} \Bigg[(g_v + g_a)^2 + \\ &\qquad (g_v - g_a)^2 \left(1 - \frac{E_R}{E_\nu}\right)^2 + (g_a^2 - g_v^2) \frac{m_e E_R}{E_\nu^2} \Bigg], \end{aligned} \tag{3.23}$$

where G_F is the Fermi constant, and

$$g_{v;\mu,\tau} = 2\sin^2\theta_W - \frac{1}{2}; \;\; g_{a;\mu,\tau} = -\frac{1}{2}, \tag{3.24}$$

for muon and tau neutrinos. In the case $\nu_e + e \to \nu_e + e$, the interference between neutral and charged current interaction leads to a significant enhancement:

$$g_{v;e} = 2\sin^2\theta_W + \frac{1}{2}; \;\; g_{a;e} = +\frac{1}{2}. \tag{3.25}$$

The neutrino-nucleus cross section in the SM reads

$$\frac{d\sigma_{\nu N}}{dE_R} = \frac{G_F^2}{4\pi} Q_v^2 m_N \left(1 - \frac{m_N E_R}{2E_\nu^2}\right) F^2(E_R), \tag{3.26}$$

where $F^2(E_R)$ is the nuclear form factor, for which we have taken the parametrisation given by Helm [23]. Q_v parametrises the coherent interaction with protons (Z) and neutrons ($N = A - Z$) in the nucleus:

$$Q_v = N - (1 - 4\sin\theta_W)Z. \tag{3.27}$$

3.7 Inelastic

[24]

The WIMP needs to have sufficient speed to interact with the nucleus and promote to an excited state (with energy separation δ)

$$\frac{1}{2}\mu_{\chi N} v^2 > \delta \tag{3.28}$$

This leads to the condition

$$v_{\min} = \sqrt{\frac{1}{2m_N\, E_R}} \left(\frac{m_N\, E_R}{\mu_{\chi N}} + \delta \right) \tag{3.29}$$

Therefore, the main effect at a given experiment is to limit the sensitivity only to a part of the phase space of the halo. This favours heavy nuclei (since they can transfer more energy to the outgoing WIMP) and can account for observation in targets such as iodine (DAMA/LIBRA) while avoiding observation in lighter ones such as Ge (CDMS)

CHAPTER 4

AXIONS

4.1 The Strong QCD Problem

The most general gauge invariant QCD Lagrangian up to dimension four reads

$$\mathcal{L} = -\frac{1}{4} G^a_{\mu\nu} G^{a,\mu\nu} + \bar{q}\left(i\gamma_\mu D^\mu - \mathcal{M}_q\right) q - \frac{\alpha_S}{8\pi}\theta G^a_{\mu\nu}\tilde{G}^{a,\mu\nu} \tag{4.1}$$

The zero temperature mass of the axion field is therefore field by non-perturbative QCD, related to the axion scale, $f_{\mathfrak{a}}$, and can be computed to be

$$m_{\mathfrak{a}}(T=0) = 5.7 \times 10^{-5} \frac{10^{-11}}{f_{\mathfrak{a}}} \ . \tag{4.2}$$

The axion potential is periodic, but it is typical to adopt a harmonic approximation

$$V(\theta) = m^2_{\mathfrak{a}}(T)\left(1 - \cos\theta\right) \approx \frac{1}{2} m^2_{\mathfrak{a}}(T)\theta^2 \ . \tag{4.3}$$

4.2 Axions production

The Peccei-Quinn (PQ) symmetry breaks at a high temperature, T_{PQ}, providing a well-known dynamical solution to the so-called strong-CP problem. In this scenario, the (complex) axion field takes a non-vanishing vacuum expectation value, which fixes one of its component, leaving just a phase, which we will call axion.

There are various production mechanisms for axions, which can be thermal or non-thermal. Which of these mechanisms dominate, strongly depends on whether the PQ temperature is higher or lower than the reheating temperature, T_R.

The axion mass arises from non-perturbative QCD effects, which are negligible at high temperatures, but become relevant at a critical time, t_1 that satisfies $m_a t_1 \approx 1$, and where the temperature of the Universe is approximately $T_1 \approx 1$ GeV.

Thermal production Axions can be produced in the plasma of the Early Universe, mainly by processes which involve quarks and gluons [25]. These processes can lead to a population of hot axions if the Peccei-Quinn axion scale is $f_a < 10^{12}$ GeV [26] (and in fact, any population of cold axions produced before this period would also thermalise). After colour confinement, the leading thermal production process is through the coupling to pions, $\pi + \pi \leftrightarrow \pi + a$ [27]. These hot axions would contribute to the universe energy density and, like in the case of neutrinos, cosmological constraints impose upper bounds on their mass (see for example Ref. [28]). I, particular, if thermally produced, axions would contribute to the effective number of relativistic degrees of freedom, which is measured to be $N_{eff} = 3.15 \pm 0.23$, leading to an upper bound on the axion mass of $m_a < 0.529$ eV [29].

A recent update of the thermal axion production can be found in Ref. **??**, which includes not only axion couplings to gluons, but also contributions from couplings to electroweak bosons.

Misalignment mechanism Cold axions can be produced in the early Universe through the so-called misalignment mechanism [30, 31, 32], also called vacuum realignment in the literature.

We can consider a toy model, where the potential for the complex field $\phi(x)$ at high temperature reads

$$V(\phi) = \frac{\lambda}{4}\left(|\phi|^2 - v_{\mathfrak{a}}^2\right)^2 , \tag{4.4}$$

Then, when the Universe cools to $T_{PQ} \sim v_{\mathfrak{a}}$ the field ϕ takes a non-vanishing vacuum expectation value in each Hubble volume

$$\langle\phi\rangle \equiv v_{\mathfrak{a}} e^{i\theta(x)} . \tag{4.5}$$

The remaining angle is related to what we will define as the axion field, $a(x)$ as

$$\mathfrak{a}(x) = v_{\mathfrak{a}}\theta(x) . \tag{4.6}$$

The axion mass plays no role for high temperatures, but when the Universe cools down to the confinement scale $T \sim \Lambda$, non-perturbative QCD corrections "tilt" the potential,

$$\tilde{V}(\theta) = m_{\mathfrak{a}}^2(T) f_{\mathfrak{a}}^2 (1 - \cos\theta) . \tag{4.7}$$

This forces the axion to "realign" (after T_{PQ} it adopted a given value of θ and now it is forced to go towards the minimum of the potential, $\theta = 0$). This also gives the axion an effective mass whose time-dependence can be calculated in terms of the low-temperature value, $m_{\mathfrak{a}}$, to be

$$m_a(T) = 0.2\, m_{\mathfrak{a}} \left(\frac{\Lambda}{f_{\mathfrak{a}}}\right)^4 . \tag{4.8}$$

The equation of motion fo rhte axion can be computed in a FRW universe, using the definition of the D'Alambertian

$$\ddot{\theta} + 3H\dot{\theta} - \frac{1}{a^2(t)}\nabla^2\theta + m_{\mathfrak{a}}^2(T(t))\sin\theta = 0 . \tag{4.9}$$

Notice that we are using $a(t)$ to denote the scale parameter.

If $T_{PQ} > T_R$ then the axion reached the PQ minimum before reheating, taking a random value for the phase, which is then fixed by cosmic expansion. This means that θ is homogeneous at QCD confinement. This implies that the spatial derivatives can be neglected and we are left with the equation of a damped harmonic oscillator (using $\sin\theta \approx \theta$ for small angles),

$$\ddot{\theta} + 3H\dot{\theta} + m_{\mathfrak{a}}^2\theta \ = 0 \ . \tag{4.10}$$

The axion mass is not relevant at early times (and therefore θ remains constant), but after a time $t_1 = 1/m_{\mathfrak{a}}(T_1(t_1))$, that is equivalent to a critical temperature of approximately 1 GeV. At this point, the axion field responds by attempting to minimise its potential, oscillating around minimum (*vacuum-realignment*). The critical time and temperature read

$$t_1 \approx 2 \times 10^{-7}\ \mathrm{s} \left(\frac{f_{\mathfrak{a}}}{10^{12}\,\mathrm{GeV}}\right)^{1/3} , \tag{4.11}$$

and

$$T_1 \approx 1\ \mathrm{GeV} \left(\frac{10^{12}\,\mathrm{GeV}}{f_{\mathfrak{a}}}\right)^{1/6} . \tag{4.12}$$

One can estimate the momentum of the resulting quanta of the axion field. Assuming a typical coupling of $f_{\mathfrak{a}} \sim 10^{-12}$, which corresponds to an axion mass of $m_{\mathfrak{a}} \sim 6\times10^{-6}$ eV, one obtains

$$p_{\mathfrak{a}}(t_1) \sim \frac{1}{t_1} \sim 10^{-9}\ \mathrm{eV} \ . \tag{4.13}$$

In other words, classical, spatially coherent oscillating fields are equivalent to a coherent state of extremely non-relativistic dark matter, i.e. CDM). Notice that these axions, once produced, are not thermalised and therefore remain as cold dark matter throughout the evolution of the Universe.

Finally, we can compute the energy density of the axion field

$$\rho = \frac{{f_{\mathfrak{a}}}^2}{2}\left(\dot{\theta}^2 + m_{\mathfrak{a}}(t)^2\theta^2\right) \ . \tag{4.14}$$

The initial energy of the axion before starting oscillating is a function of the original mis-alignment angle, θ_1,

$$\rho = \frac{{f_{\mathfrak{a}}}^2}{2} m_{\mathfrak{a}}^2(t_1)\theta_1^2. \tag{4.15}$$

When converted to a cosmological density parameter, we obtain

$$\Omega_{\mathfrak{a}}h^2 = 0.15 \left(\frac{f_{\mathfrak{a}}}{10^{12}\ \mathrm{GeV}}\right)^2 \theta_1^2. \tag{4.16}$$

Notice that, according to this equation, an axion with a scale $f_{\mathfrak{a}} \sim 10^{12}$ GeV would reproduce the cold dark matter relic density observed by the Planck satellite, assuming that the original mis-alignment is of the order of $\theta_1 \sim 1$ (for naturalness arguments). If one is willing to abandon naturalness and introduce a degree of fine-tuning in θ_1, the axion scale can be raised arbitrarily. This solution is normally referred to as "anthropic" for that reason.

REFERENCES

[1] J. Silk et al., *Particle Dark Matter: Observations, Models and Searches*. Cambridge Univ. Press, Cambridge, 2010, 10.1017/CBO9780511770739.

[2] G. Bertone and D. Hooper, *A History of Dark Matter*, *Submitted to: Rev. Mod. Phys.* (2016) , [1605.04909].

[3] V. C. Rubin and W. K. Ford, Jr., *Rotation of the Andromeda Nebula from a Spectroscopic Survey of Emission Regions*, *Astrophys. J.* **159** (1970) 379–403.

[4] V. C. Rubin, N. Thonnard and W. K. Ford, Jr., *Rotational properties of 21 SC galaxies with a large range of luminosities and radii, from NGC 4605 /R = 4kpc/ to UGC 2885 /R = 122 kpc/*, *Astrophys. J.* **238** (1980) 471.

[5] A. Bosma, *21-cm line studies of spiral galaxies. 2. The distribution and kinematics of neutral hydrogen in spiral galaxies of various morphological types.*, *Astron. J.* **86** (1981) 1825.

[6] T. S. van Albada, J. N. Bahcall, K. Begeman and R. Sancisi, *The Distribution of Dark Matter in the Spiral Galaxy NGC-3198*, *Astrophys. J.* **295** (1985) 305–313.

[7] R. Gavazzi, C. Adami, F. Durret, J.-C. Cuillandre, O. Ilbert, A. Mazure et al., *A weak lensing study of the Coma cluster*, *Astron. Astrophys.* **498** (2009) L33, [0904.0220].

[8] F. Zwicky, *Die Rotverschiebung von extragalaktischen Nebeln*, *Helv. Phys. Acta* **6** (1933) 110–127.

[9] F. Zwicky, *On the Masses of Nebulae and of Clusters of Nebulae*, *Astrophys. J.* **86** (1937) 217–246.

[10] J. M. Kubo, A. Stebbins, J. Annis, I. P. Dell'Antonio, H. Lin, H. Khiabanian et al., *The Mass Of The Coma Cluster From Weak Lensing In The Sloan Digital Sky Survey*, *Astrophys. J.* **671** (2007) 1466–1470, [0709.0506].

[11] M. Markevitch, A. H. Gonzalez, D. Clowe, A. Vikhlinin, L. David, W. Forman et al., *Direct constraints on the dark matter self-interaction cross-section from the merging galaxy cluster 1E0657-56*, *Astrophys. J.* **606** (2004) 819–824, [astro-ph/0309303].

[12] D. Clowe, M. Bradac, A. H. Gonzalez, M. Markevitch, S. W. Randall, C. Jones et al., *A direct empirical proof of the existence of dark matter*, *Astrophys. J.* **648** (2006) L109–L113, [astro-ph/0608407].

[13] S. D. McDermott, H.-B. Yu and K. M. Zurek, *Turning off the Lights: How Dark is Dark Matter?*, *Phys. Rev.* **D83** (2011) 063509, [1011.2907].

[14] C. Kouvaris, *Composite Millicharged Dark Matter*, *Phys. Rev.* **D88** (2013) 015001, [1304.7476].

[15] A. D. Dolgov, S. L. Dubovsky, G. I. Rubtsov and I. I. Tkachev, *Constraints on millicharged particles from Planck data*, *Phys. Rev.* **D88** (2013) 117701, [1310.2376].

[16] E. Del Nobile, M. Nardecchia and P. Panci, *Millicharge or Decay: A Critical Take on Minimal Dark Matter*, *JCAP* **1604** (2016) 048, [1512.05353].

[17] S. Tulin, H.-B. Yu and K. M. Zurek, *Resonant Dark Forces and Small Scale Structure*, *Phys. Rev. Lett.* **110** (2013) 111301, [1210.0900].

[18] P. Gondolo and G. Gelmini, *Cosmic abundances of stable particles: Improved analysis*, *Nucl. Phys.* **B360** (1991) 145–179.

[19] M. Srednicki, R. Watkins and K. A. Olive, *Calculations of Relic Densities in the Early Universe*, *Nucl. Phys.* **B310** (1988) 693.

[20] T. Nihei, L. Roszkowski and R. Ruiz de Austri, *Exact cross-sections for the neutralino slepton coannihilation*, *JHEP* **07** (2002) 024, [hep-ph/0206266].

[21] L. J. Hall, K. Jedamzik, J. March-Russell and S. M. West, *Freeze-In Production of FIMP Dark Matter*, *JHEP* **03** (2010) 080, [0911.1120].

[22] F. Mayet et al., *A review of the discovery reach of directional Dark Matter detection*, *Phys. Rept.* **627** (2016) 1–49, [1602.03781].

[23] R. H. Helm, *Inelastic and Elastic Scattering of 187-Mev Electrons from Selected Even-Even Nuclei*, *Phys. Rev.* **104** (1956) 1466–1475.

[24] D. Tucker-Smith and N. Weiner, *Inelastic dark matter*, *Phys. Rev.* **D64** (2001) 043502, [hep-ph/0101138].

[25] M. S. Turner, *Thermal Production of Not SO Invisible Axions in the Early Universe*, *Phys. Rev. Lett.* **59** (1987) 2489.

[26] E. Masso, F. Rota and G. Zsembinszki, *On axion thermalization in the early universe*, *Phys. Rev.* **D66** (2002) 023004, [hep-ph/0203221].

[27] S. Chang and K. Choi, *Hadronic axion window and the big bang nucleosynthesis*, *Phys. Lett.* **B316** (1993) 51–56, [hep-ph/9306216].

[28] A. Melchiorri, O. Mena and A. Slosar, *An improved cosmological bound on the thermal axion mass*, *Phys. Rev.* **D76** (2007) 041303, [0705.2695].

[29] E. Di Valentino, E. Giusarma, M. Lattanzi, O. Mena, A. Melchiorri and J. Silk, *Cosmological Axion and neutrino mass constraints from Planck 2015 temperature and polarization data*, *Phys. Lett.* **B752** (2016) 182–185, [1507.08665].

[30] J. Preskill, M. B. Wise and F. Wilczek, *Cosmology of the Invisible Axion*, *Phys. Lett.* **B120** (1983) 127–132.

[31] L. F. Abbott and P. Sikivie, *A Cosmological Bound on the Invisible Axion*, *Phys. Lett.* **B120** (1983) 133–136.

[32] M. Dine and W. Fischler, *The Not So Harmless Axion*, *Phys. Lett.* **B120** (1983) 137–141.